SOIL CO_2 EMISSIONS: A PROXY FOR HEAT AND MASS FLOW ASSESSMENT, ROTOKAWA, NEW ZEALAND.

[1*]Bloomberg, S., [2]Rissmann, C., [3]Mazot, A., [4]Werner, C., [1]Horton, T., [1]Oze, C., [1]Gravley, D., and [1]Kennedy, B.

[1]University of Canterbury, 20 Kirkwood Avenue, Ilam 8041, NZ

[2]Environment Southland, 202 Price Road, Waikiwi 9810, NZ

[3]GNS Science, Wairakei Research Centre, Taupo, NZ

[4]Alaska Volcano Observatory, 4200 University Drive, Anchorage, AK

[*]simonhbloomberg@gmail.com

Keywords: *Rotokawa, Soil Gas, Gas Carbon Isotopes, Geochemistry, Carbon Dioxide Flux, Sequential Gaussian Simulation, Graphical Statistical Approach.*

ABSTRACT

The quantification of the heat and mass flow between deep reservoir(s) and the surface is a significant challenge to the sustainable development and exploration of magma-hydrothermal systems. Here, we use high resolution measurement of carbon dioxide (CO_2) flux and heat flow at the land surface to characterize the mass (CO_2 and steam) and heat released from the magma-hydrothermal systems. Statistical and isotopic characterization of background sources of CO_2 flux is utilized to reduce the level of uncertainty when deriving mass (emissions) and heat flow estimates from high temperature reservoirs.

The soil gas and heat flow survey of the Rotokawa thermal area consisted of ~2,900 direct measurements of CO_2 flux and soil temperature, and 60 soil gas carbon isotopes samples. Results indicate a total CO_2 emission rate of 633 ± 16 t d^{-1} (2.5 km^2) for Rotokawa. The measured thermal energy release at the Rotokawa thermal area was 37MW_t and by combining the magmatic-hydrothermal sourced CO_2 emission (constrained using stable isotopes) with reservoir H_2O:CO_2 concentration ratios and the enthalpy of evaporation; the projected reservoir mass flow was 120 Kg s^{-1} and the heat flow was 314 MW_t. CO_2 emissions are higher than previously published values by up to 570 td^{-1} at Rotokawa and while mass and heat flow values are within historical predictions. Paired assessment of the CO_2 source using stable isotopes and statistical analysis of the CO_2 flux has reduced the uncertainty when constraining the magma-hydrothermal CO_2 emission from the reservoirs and has implications for blind geothermal system exploration.

1. INTRODUCTION

Heat and mass transfer through magmatic-hydrothermal systems in the Taupo Volcanic Zone (TVZ) of New Zealand has been evaluated using a variety of surface geophysical, geochemical and geological techniques (*Donaldson & Grant*, 1978; *Lyon & Hulston*, 1984; *Bibby et al.*, 1995b; *Seward & Kerrick*, 1996; *Rowland & Sibson*, 2004). Surveys of magmatic-hydrothermal systems are used to (1) better quantify the contribution of CO_2 emissions to the global carbon cycle (cf. *Seward & Kerrick*, 1996; *Mörner & Etiope*, 2002), (2) identify temporal changes for volcano monitoring purposes (*Chiodini et al.*, 1998, 2005, 2008; *Mazot et al.*, 2011) and (3) assess the potential for geothermal power. As the measurement of CO_2 flux and its use as a proxy for total heat and total mass transfer has improved, the technique now has applications in geothermal exploration and field management (*Sheppard et al.*, 1990; *Werner et al.*, 2004; *Werner & Cardellini*, 2006; *Werner et al.*, 2008; *Rissmann et al.*, 2011, 2012).

Magmatic-hydrothermal systems can be divided into non-volcanic and volcanic types (*Kerrick*, 2001; *Mörner and Etiope*, 2002). The CO_2 emission from actively degassing volcanoes (i.e. Vulcano; *Chiodini et al.*, 1998) is variable over a wide range of magnitudes. Diffuse degassing of non-volcanic systems (i.e. Reykjanes; *Fridriksson et al.*, 2006), when properly constrained, produces a similar range of emissions to active volcanoes or in some cases higher emissions as exemplified in New Zealand (cf. *Seward & Kerrick*, 1996; *Werner et al.*, 2004; *Werner & Cardellini*, 2006; *Rissmann et al.*, 2012). As such, when calculating total CO_2 emissions for convergent plate boundary volcanism (like the TVZ), inclusion of non-volcanic systems can only improve the accuracy of these carbon-cycle fluxes.

Here we present a high resolution soil gas flux and heat flow survey for Rotokawa (RK) thermal area, a developed high temperature (>200°C) non-volcanic geothermal system within the TVZ. In addition to emission estimates, we also determined the sources of CO_2 at RK using cumulative probability plots and stable isotopic analysis of ^{13}C and by comparison with CO_2 flux and soil temperature. Total heat flow (MW_t), total mass flow (Kg s^{-1}) and soil gas emission rates (td^{-1}) are quantified for each survey along with detailed maps of

the spatial extent and magnitude of soil gas flux and heat flow. Normalized to total thermal area and total emission rates are contrasted with values reported for fields within the TVZ and worldwide (*Mörner and Etiope*, 2002*; Werner and Cardellini*, 2006*; Rissmann*, 2010*; Inguaggiato et al.*, 2012) and spatial maps of surface flux and heat flow are used to infer structural controls to fluid flow. Finally, a comparison is made between the observed CO_2 and derived heat flow estimates from this study and previously published estimates.

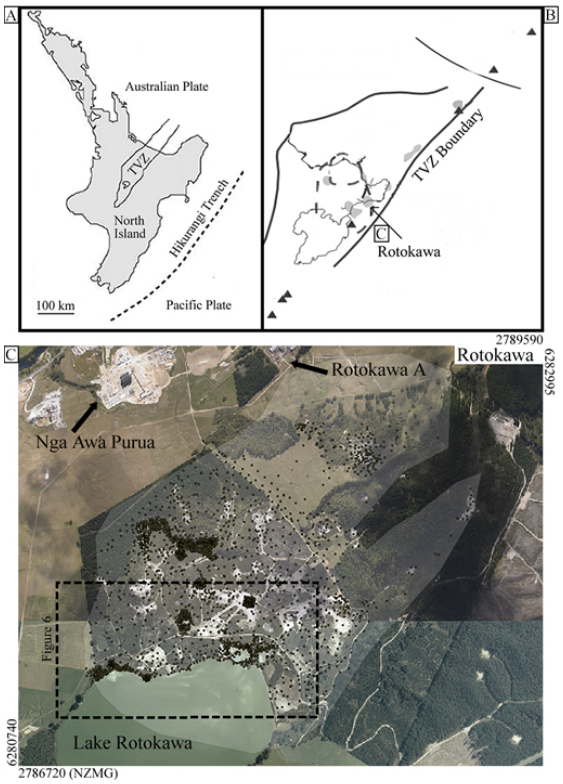

Figure 1: A) Map of the North Island, NZ. B) Close-up of the TVZ. C) Aerial of the Rotokawa Thermal Area (shaded grey) & Surrounds, with sample locations as black points.Figure 6 blow up outlined by black dash.

2. GEOLOGICAL SETTING OF ROTOKAWA

The geothermal system at RK fits within an 18-26 km^2 resistivity boundary defined by surveys completed in the 1960's and 1980's (*Hedenquist et al.*, 1988). The principal thermal feature is a warm (~24°C, surface) acid (pH ≈2.2) lake (Lake Rotokawa) with an area of ~0.62 km^2. To the north of the lake lies the RK thermal area with numerous thermal features (steaming ground, hot pools, sink holes, sulphur banks, hydrothermal eruption craters and fumaroles; *Krupp & Seward*, 1987). *Collar and Browne* (1985) noted that the hydrothermal explosions craters are less than 20,000 years old and structurally aligned in a NE/SW orientation coincident with deep field faults (*Winick et al.*, 2011). The RK thermal area has been extensively modified by historic sulphur mining and thermal features have been created where the land surface was excavated and/or a confining impermeable cap removed.

Two geothermal power stations generate from the geothermal reservoir (Figure 1), Rotokawa A ($34MW_e$) and Nga Awa Purua ($140\ MW_e$). The maximum fluid temperature is ~320°C, recorded within the Rotokawa andesite deep reservoir rock (*Hedenquist et al.*, 1988). A plume of two-phase fluid flows from the deep reservoir through to the surface along a deep field fault and mixes in a shallow aquifer near the lake (*Winick et al.* 2011). A local confining layer (a volcaniclastic lake deposit rich in clays, 'the Huka Falls Formation') has been removed in the thermal area by both hydrothermal eruptions and dissolution, this has opened the permeability for mixed neutral chloride and acid sulphate fluid to flow through hot springs and steaming ground (*Krupp & Seward*, 1987).

3. METHODS & MATERIALS

3.1 Soil gas flux and temperature measurements

Soil gas flux of CO_2 (φCO_2) and H_2S (φH_2S) and soil temperatures were measured using the accumulation chamber method (*Chiodini et al.*, 1998; *Werner et al.*, 2000; *Lewicki et al.*, 2005; *Rissmann et al.*, 2012*)* with a West Systems accumulation chamber and LICOR LI-820 infrared gas analyser for CO_2 (*Welles et al.*, 2001) that is calibrated annually and has a sensitivity range of 0-20,000 ppm. *Evans et al.*, (2001) and *Giammanco et al.* (2007) both tested the accuracy of the accumulation chamber technique with a series of replicate measurements of known CO_2 effluxes through a synthetic soil. *Evans et al.* (2001) found that the accumulation chamber measured a mean flux at -12.5% below the imposed fluxes while *Giammanco et al.* (2007) reported an average measurement error of ±5% that they attributed to natural variability, and recorded a mean difference between measured and imposed fluxes of +5%. We used an identical system to that assessed by *Giammanco et al.* (2007) and assume a similar mean measurement error of approximately +5%. The fieldwork was undertaken in dry and stable conditions in order to minimize the influence of rain, wind, soil humidity and atmospheric pressure changes on φCO_2. Sampling of H_2S flux was limited at times due to the poor response of the chemical sensor. Additionally, the purge time (<2 min) between consecutive measurements did not enable the H_2S sensor to recover from previous high measurements. Due to the limited φH_2S measurements, 'flux' in this study relates to φCO_2 unless otherwise stated.

Soil temperatures were measured to 10 cm depth within ~0.1m of the accumulation chamber footprint using a Yokogawa TX-10 digital thermometer and a K-type thermocouple (measurement accuracy ±0.5°C). Ambient air temperature and barometric pressure were logged at the start of each day and after each 25 consecutive measurements of flux and soil temperature.

The flux survey design used a systematic sampling approach (quasi-regular grid spacing of 10 m - 25 m) coupled with an adaptive cluster component (e.g. *Thompson,* 1990). Deviation from the systematic sampling pattern was guided by sensory cues such as ground alteration and odour with the adaptive component initiated when a measurement exceeded the estimated background flux level (>90 g m^{-2} d^{-1}, ≥ ambient T°C) at which point the resolution increased to 5 m spacing (Figure 1).

Two fumaroles were sampled to find the H_2O:CO_2:H_2S concentration in steam. They were sampled using the same setup from Rissmann (2010) and analysed in the same laboratory.

3.2 Carbon isotopic analysis of soil gas

In order to define the magma-hydrothermal source, we analysed the stable isotopic composition of CO_2 ($\delta^{13}C_{CO2}$) by collecting a gas sample concurrently with soil gas flux measurements in the West Systems accumulation chamber. A 5 mL syringe was used to pierce a rubber septum on top of the chamber. A gas sample was drawn and emptied into a helium filled 10mL exetainer vial capped with a pierceable butyl rubber septum. A fresh needle and syringe is used for each sample. Samples were taken direct from the chamber to prevent mixing and contamination from other possible sources of CO_2 (*Chiodini et al.*, 2008).

Values of $\delta^{13}C_{CO2}$ were determined using a Thermo Scientific GasBench II connected to a Delta V Plus gas isotope ratio mass spectrometer under continuous flow conditions within 48 hours of collection of the soil gas CO_2. A total of 60 samples were analysed. Stable oxygen and carbon isotopic compositions are accurate to <0.10 ‰ based on replicate analysis of NBS-19 and NBS-22 certified reference materials.

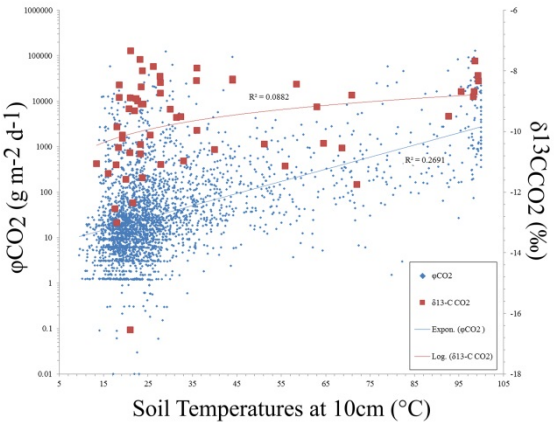

Figure 2: Plot of Soil Temperature vs. φCO_2 vs. $\delta^{13}C_{CO2}$

3.3 Data Analysis

Raw φCO_2 and φH_2S data were converted from ppm s^{-1} to g m^{-2} d^{-1} to account for the ambient temperature, atmospheric pressure and the area and volume of the accumulation chamber. Additionally, raw soil temperature values were converted from °C to W (watts) m^{-2} (following the procedure discussed in the next section).

Interpolation of the unsampled area was modelled using the sequential Gaussian simulation (sGs) algorithm within the WinGsLib software toolbox (*Deutsch & Journel*, 1998), and following the methods of *Cardellini et al.* (2003). The direct measurement data sets for φCO_2 and soil temperature/heat flow (Figure 2) were declustered to remove the sample bias induced by using adaptive clustering and then normally scored prior to interpolation. Each simulation ran for 500 realisations at 10 m cell size using variogram models (Figure 3b). Post-processing of the 500 flux grid realizations included computation of mean flux and the probability of high and low fluxes at each location. Emission rates (t d^{-1}) for each realization were calculated by summing the simulated flux across the grid and multiplying by the grid area using the back-transformed data. The mean and standard deviations of the emission rates were computed from the 500 realizations conducted for each grid area.

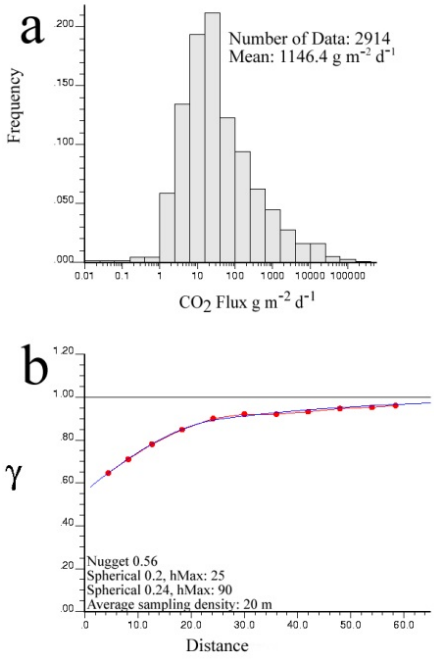

Figure 3:Histogram and variogram from the raw data

CO_2 flux and soil temperature models were mapped as 2D pixel plots obtained from a point-wise linear averaging of the 500 realizations (E-type estimation) of each site. Finally, 2D pixel plots of the different flux populations were modelled using various flux cut-offs, set according to the population thresholds identified from isotopic values and log cumulative probability plots of φCO_2. The spatial distribution in soil temperatures were

also modelled spatially through sGs realizations using the method described for soil CO_2 flux.

As diffuse CO_2 flux from the soil may originate from multiple sources (i.e. soil-respired, atmospheric, and/or magmatic), flux data was evaluated using *Sinclair's* (1974) method by: 1) plotting geochemical data on a log-normal probability plot with a Gaussian distribution (cumulative probability) and 2) then separating the dataset into populations. Log cumulative probability plots were also applied to $\delta^{13}C_{CO2}$ and φCO_2, respectively, in attempt to better resolve the contribution of soil-respired or background sources to the total CO_2 emission occurring at RK (Figure 4).

3.4 Heat and mass flow from soil temperature

Soil temperature measurements were taken (2914) at a depth of ~10cm. If the boiling point temperature (98.7°C) was reached before 10cm this was noted. Soil temperature measurements were converted to equivalent heat and mass flow values using soil-temperature heat flow functions (cf. *Rissmann et al.*, 2012; *Dawson*, 1964 & *Fridrikkson et al.*, 2006.).

3.5 Heat and mass flow and emissions calculations from CO_2 flux

An alternative measure of the steam mass flow (or heat release) from the high temperature reservoirs at both fields is made by multiplying the total CO_2 emission rate by the representative concentration ratio of CO_2 in steam (H_2O:CO_2) supplying surface thermal activity (*Chiodini et al.*, 2005; *Fridriksson et al.*, 2006):

$$F_{stm(CO_2)} = F_{CO_2} \cdot \frac{[H_2O]}{[CO_2]} \quad (1)$$

where F_{CO_2} is the total flux of CO_2 in g s^{-1}, $\frac{[H_2O]}{[CO_2]}$ is the concentration ratio in g, and $F_{stm(CO2)}$ is the steam mass flow in g s^{-1}. In this way we can calculate the quantity of steam mass flow that is condensed within the subsurface by comparing $F_{stm(CO2)}$ with the value from heat flow through soil (*Fridriksson et al.*, 2006).

An equivalent heat flow (H_s) can be calculated for the steam mass flow ($F_{stm(CO2)}$) derived from Equation (1) using:

$$Hs = F_{stm(CO_2)} \cdot h_{s,100°C} \quad (2)$$

where $Fstm(CO_2)$ is from Equation (1), and is the steam flux in g s^{-1}, and $h_{s,100°c}$ is the enthalpy of steam at 100°C (2676 kJ/kg) and Hs is the heat flow in Watts (*Fridriksson et al.*, 2006).

4. RESULTS

4.1 Diffuse soil gas fluxes, stable isotopes and soil temperatures

Diffuse soil CO_2 fluxes range from <1 to 127,808 g m^{-2} d^{-1} from 2,914 direct measurements (Figures 1 and 2). Across a 2.5 km^2 area of the RK field the arithmetic and declustered means were 1146 g m^{-2} d^{-1} and 234 g m^{-2} d^{-1}, respectively, while the sGs modelling produced a mean of 246 g m^{-2} d^{-1}. The coefficient of variation is 8.4 with the population being approximately log-normal with a positive skew which is consistent with a CV >1 for non-normal data (Figure 3a). The total CO_2 emission estimates is 633 t d^{-1} for the 2.5 km^2 modelled area.

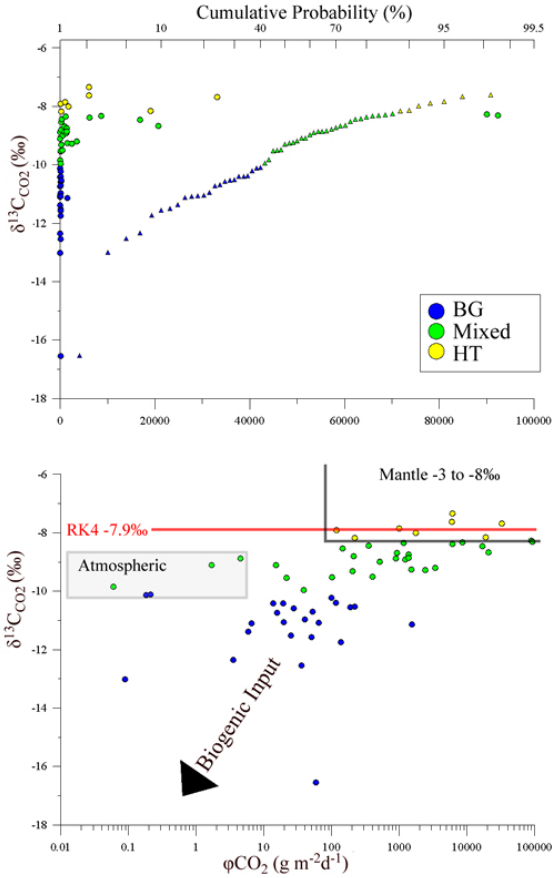

Figure 4: Plot of $\delta^{13}C_{CO2}$ vs. φCO_2 and Cumulative probability, Filled triangles are plotted on the top axis, while filled circles are plotted on the bottom axes.

Shallow soil temperatures (Figure 2) ranged from 9 °C to boiling point (98.7°C at 350m ASL.). The arithmetic and declustered means were 29.5 and 23.4 °C. The relationship between CO_2 and soil temperature has an r^2 value of 0.26.

$\delta^{13}C_{CO2}$ values (‰) range from -16.5 to -7.3 (n=60). The relationships between $\delta^{13}C_{CO2}$ with soil temperature (Figure 2) and φCO_2 (Figure 4) have an r^2 value 0.08 and 0.3, respectively. The mean for the whole dataset is -9.7 ± 0.4 ‰.

4.2 φH2S and relationships with φCO2

Samples of φH_2S from 121 sites range from 0.2 to 156 g m^{-2} d^{-1}. The r^2 value for CO_2 and H_2S is 0.65 (Figure 5) though for H_2S and soil temperature it is 0.25. In Figure 5 we plot the fluxes comparatively and find a threshold

relationship where φH_2S is below detection until φCO_2 values exceed a threshold of ~100 g $m^{-2}d^{-1}$ at which point both gaseous species are detected.

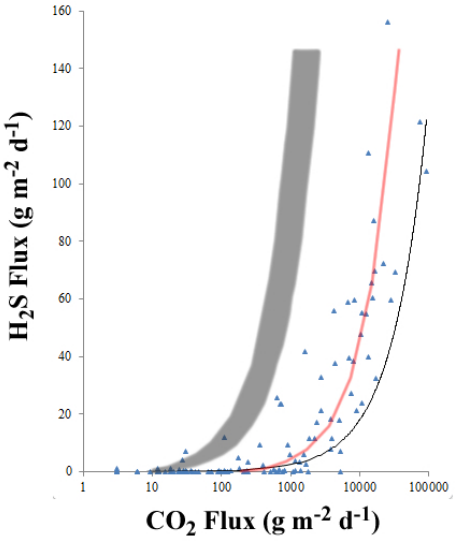

Figure 5: Distribution of the acid soil gases at RK. The solid grey bar is the estimated fluxes based on fumarolic gas ratios (max=4.5, min=9.6). The red line is the average diffuse CO2:H2S ratio of 241. The black line is a trend line (power) where r^2=0.65

Two fumarole samples were used to calculate the CO_2:H_2S ratio of surface advective steam flow (pipe flow). The range of the ratios (Figure 5) provides an estimate of the distribution of the gas composition for advective degassing. While a few of the soil fluxes fall within this range most of the data show a higher CO_2:H_2S gas flux ratio.

The CO_2:H_2S ratio for the fumaroles has a mean of 7.9 while the mean ratio for significant soil gas flux is 241, historic gas data from wells puts the ratio around 45 (*Hedenquist et al.* 1988).

4.3 Heat and mass flow based on soil temperature measurements

Using the respective heat flow equations (*Rissmann et al.*, 2012) the soil temperature data was modelled with sGs and converted into a total megawatt (MW_t) value. Heat flow measurements ranged between 0.03 – 4526 with a mean of 15 W m^{-2}. The total heat flow through soil is estimated to be 37 ± 1.5 MW_t, which is then used to find the equivalent steam mass flow of 1267 ± 23 t d^{-1}.

4.4 Heat and mass flow calculated from CO_2 degassing

Calculating the total heat input was accomplished using Equations (1) and (2), where the total magmatic-hydrothermal CO_2 flux (614 t d^{-1}, see discussion) is multiplied by the H_2O:CO_2 ratio in the deep fluid (61g kg^{-1} or 1:16.6; *Hedenquist et al.*, 1988), to give a steam flux ($F_{stm(CO2)}$) of 10,204 ± 255 t d^{-1} H_2O. From this value a heat flow of 315 ± 8 MW_t is calculated. Total mass flow is calculated by combining the 10,204 t d^{-1} H_2O and 614 t d^{-1} CO_2 to a value of 125 ± 3 Kg s^{-1}, which is in good agreement with previously published values for total mass flow of 144 and 105 Kg s^{-1} (*Seward & Kerrick*, 1996; *Bowyer & Holt*, 2010).

5. DISCUSSION

5.1 Defining the multisource nature of CO_2

In order to use total CO_2 emission values for the estimation of heat and mass flow from a magmatic-hydrothermal system it is necessary to define the contributions from the different φCO_2 sources. To produce these values, any contribution from non-magmatic-hydrothermal sources (atmospheric or soil-respired/biogenic in this case) must be removed from the calculation. Two methods were employed in this study: (1) the GSA method of breaking the flux data into populations (*Chiodini et al.*, 1998) and (2) the use of stable isotopic analysis of the φCO_2 to identify source components (*Chiodini et al.*, 2008).

When using GSA, we assume that low flux populations (<30 g m^{-2} d^{-1}) are background for a system in which permeability is constant. The heterogeneity in permeability at our field sites and the large volume and pervasiveness of magma-hydrothermal φCO_2 population means this method, on its own, may not fully constrain the source populations. The latter became evident when stable isotope analysis was paired with flux data and there were fluxes which had magma-hydrothermal $\delta^{13}C_{CO2}$ values (Figure 4). While GSA does not fully constrain a source, it can illustrate the natural variations within the total flux population, which makes it feasible as a method for the quick estimation of a source's contribution. However, as noted by others the partitioning procedure does not result into a unique solution (*Chiodini et al.*, 2008).

While the GSA populations are defined by inflections in the slope and therefore span defined sections (Figure 4), the stable isotope analysis has provided source populations which in some instances span the whole range of fluxes (Figure 4). The paired use of stable isotopes and the GSA to isolate the source populations is the method used in this study, as it was in *Chiodini et al.* (2008). The threshold was set at <30 g m^{-2} d^{-1}.

5.2 Analysis of soil $\delta^{13}C_{CO2}$

The maximum $\delta^{13}C_{CO2}$ of the φCO_2 (-7.3‰) is consistent with the findings of *Hedenquist et al.* (1988) for RK4 (gas phase CO_2 in the well, -7.9‰) and for the Rotokawa fumarole (vent, -7.8‰), and indicates that the deep carbon source is indistinguishable from the soil CO_2 samples taken within the thermal area. The contribution to soil CO_2 from different sources can be observed in Figure 4 where the maximum isotopic value of -7.3‰ is defined as the magmatic-hydrothermal end-member and

the minimum value of -16.5‰ is the background end member. A large area of the thermal area at RK is vegetated by C3 plants (e.g. prostrate Manuka) which yield a $\delta^{13}C_{CO2}$ of -24‰ (*Amundson et al.*, 1998) during decomposition and root respiration. The other minor contributions to φCO_2 are from litter and humus decomposition and infiltration of the atmospheric CO_2, both of which minimally contribute if there is active root respiration occurring (*Amundson et al*., 1998).

The average $\delta^{13}C_{CO2}$ value from the sampling is -9.7 ± 0.4‰ though no spatial correlations can be drawn here due to the biased sampling design. High water tables can reduce anomalous soil temperatures while not affecting the flux (Figure 6a and b), therefore the correlation between soil temperature and $\varphi CO_2/\delta^{13}C_{CO2}$ are limited (Figure 2).

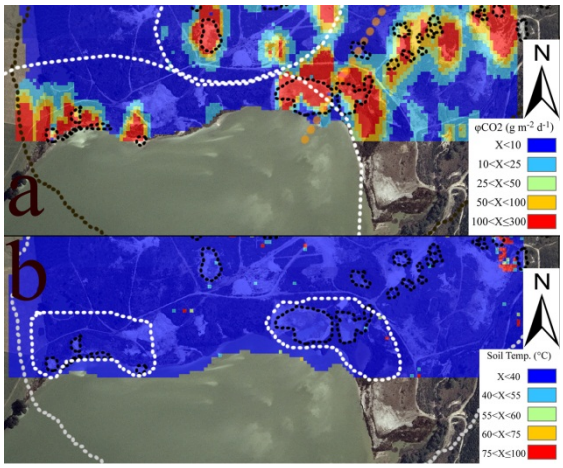

Figure 6: Pixel plots of the sGs modelled a) φCO_2 and b) soil temperatures, showing the temperature anomolies next to Lake Rotokawa (white dash in b)

In many areas of low flux (<100 g m^{-2} d^{-1}), $\delta^{13}C_{CO2}$ signatures (>-8‰, Figure 4) were relatively positive suggesting that permeability is constraining the soil gas flux of magma-hydrothermal CO_2, as opposed to the low fluxes from soil-respired or atmospheric CO_2. For example, the lowest measured $\delta^{13}C_{CO2}$ signature is -16.5‰ and corresponds to a φCO_2 of 59 g m^{-2} d^{-1}. If the origin of the isotopically lightest soil-respired CO_2 is -24‰, then the -16.5‰ value is significantly mixed with hydrothermally-sourced CO_2. A flux of 59 g m^{-2} d^{-1} is at least 2 to 4 times as large as natural soil respired background (15 – 30 g m^{-2} d^{-1}) measured for un-irrigated pasture in the Taupo Volcanic Zone (pers. comm. Rissmann, 2012). This suggests a significant hydrothermal CO_2 input even at low flux sites (<100 g m^{-2} d^{-1}) and, therefore, the dominant control on flux is permeability. These types of correlations show that $\delta^{13}C_{CO2}$ measurements have potentially profound implications for the discovery of blind geothermal systems concealed by low CO_2 fluxes.

5.3 Soil Gas Emissions

Soil gas flux measurements at RK geothermal field cover a wide range (<1 to 127,808 g m^{-2} d^{-1}) with a significant throughput of magmatic-hydrothermal CO_2 within regions of the thermal ground. The thermal area at RK (defined by resistivity and vegetation analysis; Figure 1, 2.5km^2) has a modelled emission of 633 ± 16td^{-1}. This emission rate is purely for soil zone CO_2 and does not include measurement of gaseous efflux from any other thermal features at RK (Lake Rotokawa, hot pools, fumaroles, mud pools). Applying the magmatic-hydrothermal CO_2 threshold to this total emission value reduces the product to an emission of 614 ± 15 t d^{-1}.

Historically, measurements at RK indicated a small CO_2 emission; *Seward and Kerrick* (1996) calculated a total CO_2 emission from RK to be ~55 t d^{-1} based on a total mass flow of 144 Kg s^{-1} and a concentration ratio of kgH_2O:4.4gCO_2. This H_2O:CO_2 ratio was the key factor in their underestimation of the CO_2 flux. The high spatial resolution of direct measurements in this study has produced a similar total mass flow to the *Seward and Kerrick* (1996) value of 144 Kg s^{-1}; however, our CO_2 value of 614 ± 15 t d^{-1} indicates that the *Hedenquist et al.* (1988) H_2O:CO_2 concentration ratio of kgH_2O:61gCO_2 is more accurate.

5.4 Structural and permeability controls on CO_2 emissions

Figure 7 shows the significant flux (>300 g m^{-2} d^{-1}) anomalies are quasi-circular in nature but become more diffuse and broadly distributed at lower flux rates. There is a clear correlation of surface thermal features with areas of high flux. Areas of thermal features are concentrated either along lineations that trend NE or within the bounds of historic hydrothermal eruption craters (Figure 7). The highest flux values occur along the lake shore and coincide with lower average soil temperatures (<50°C, Figure 2) indicating some decoupling of steam flow likely due to high water tables adjacent to the lake (Figure 6b). To the north and northwest greater coupling between heat flow (high soil temperatures) and CO_2 flux indicates less scrubbing of the steam phase by cooler lake waters. The active thermal area has been mapped previously using resistivity boundaries and thermal anomalies (Figure 7; *Gregg*, 1958; *Hochstein et al*, 1990) and the flux map does not produce any significant flux or thermal anomalies outside of this mapped boundary.

The location of the thermal area at RK coincides with a series of historic hydrothermal explosion craters. The largest of which is the site of Lake Rotokawa (*Collar and Browne*, 1985). Most diffuse degassing is coupled to explosion craters and boiling acidic SO_4-Cl springs and steaming ground and decreases rapidly in magnitude with distance away from them. Of note there is a major anomaly along a feature attributed to a hydrothermal eruption crater rim by *Krupp and Seward* (1987) which runs E-W for 300m across the thermal area (Figure 7).

Lake Rotokawa, a depression caused by a hydrothermal eruption crater, has a large recharge of CO_2-unsaturated

meteoric waters to depths of >200m. This depth is enough to dissolve any fluxing CO_2 and no visible bubbles are present mid lake. Close to the lake shore it shallows steeply and so that water column can be saturated in CO_2 and any incoming flux will degas at the surface as bubbles. Some of the highest measured φCO_2 is located close to the shore line which is indicative of significant permeability related to the rim of a large hydrothermal eruption crater (*Collar & Browne,* 1985; *Krupp and Seward,* 1987).

Historic mining of sulphur has also affected the topography of the thermal area by creating depressed surfaces which now intersect with the water table allowing hot springs and steaming ground to form.

Deep field faulting can cause hot spots of high permeability that allows boiling fluids to rise (*Rowland and Sibson,* 2004; *Rissmann et al.,* 2011). There is a large field fault running through the middle of the RK thermal area, the Central Field Fault (CFF, Figure 7) of *Winick et al.* (2011), which increases the number of diffuse degassing structures near historic eruptions craters which appear to focus along its strike. The magnitude of the gas fluxes in the vicinity of these craters and along the strike of the CFF suggests a deep-seated connection between surface eruption craters and the CFF which is likely channelling fluids from depth.

5.5 A sulphur budget for Rotokawa

In order to produce a sulphur budget, the CO_2 emissions associated with all fluxes in excess of 100 g m^{-2} d^{-1} are multiplied by the molar CO_2:H_2S ratio for the soil zone to produce a total H_2S emission from diffuse soil degassing of 2.6 t d^{-1}. Two previous study from Lake Rotokawa found 84.3 and 10.4 t d^{-1} SO_4^{2-}, which equates to 29.9 and 3.67 t d^{-1} H_2S (multiplying by the molar weight ratio, sulphur oxidation), respectively (*Krupp and Seward,* 1987; *Hedenquist et al.,* 1988; *Werner et al.,* 2008). This gives a minimum total surface sulphur emission for RK of 6 t d^{-1} with a minimum total emission of H_2S from the reservoir at 80 t d^{-1} (multiplying the total CO_2 by the CO_2:H_2S fumarole ratio). The loss of ~74 t d^{-1} of H_2S within the subsurface is attributed to being scrubbed by shallow groundwater and/or precipitates (as elemental S) before reaching the surface of the field. This can be reconciled with the large (2.6 Mt) sulphur lode found within cm's of the surface at RK. At 6 t d^{-1} the lode would take a minimum of 1150 years to accumulate or 100 years at 80 t d^{-1}. *Krupp and Seward* (1987) estimated the deposit accumulated at 5 t d^{-1} over 1420 years which could indicate that RK has been emitting similar rates of H_2S and, therefore, CO_2 for over 6,000 years. Due to the Taupo pumice alluvium capping the area these deposits are now at depth and the current rate of deposition is greatly reduced and is spatially confined to Lake Rotokawa (*Krupp & Seward.,* 1987).

As φH_2S occurs in background concentrations until φCO_2 becomes advective (Figure 5). Based on interpretations of this phenomenon by *Werner et al.* (2008) it is assumed that a similar process is occurring at RK, where during low CO_2 fluxes, diffusion is the main mechanism and H_2S is removed, but when there is high CO_2 flux some H_2S can reach the surface.

5.6 Heat flow from CO2 emissions

Soil temperature derived heat flow data displays lower observed heat flow than that estimated from CO_2 emissions. The discrepancies in heat flow values likely reflect the condensation of 88% (37 and 314 MW_t, RK) of the steam phase within shallow groundwater that overlies the high temperature reservoirs.

Fridriksson et al. (2006) report the condensation of 87% of steam mass flow for the Reykjanes thermal area in Iceland as based on the discrepancy between observed heat flow and heat flow estimated from CO_2 flux, which matches closely with the discrepancy at RK. The system at RK probably loses heat laterally (like Reykjanes) to cooler groundwater inflows triggering condensation of rising hydrothermal fluids, as well as having a deeper heat source (4-5km; *Winick et al.,* 2011).

Historic heat flow studies at RK presented in *Hedenquist et al.* (1988) and *Seward and Kerrick* (1996) put the thermal energy release between 210 and 236MW_t but also report numbers as high as 600MW_t. *Bibby et al.* (1995b) estimated a total heat outflow for RK of 300 MW_t which is close to this study's value of 315 ± 8 MW_t. These historic values of heat flow are all based on chloride measurements, which might be less conservative when it comes to fluid-rock interaction (*Bibby et al.,* 1995a) and also less mobile than CO_2. For groundwater having reached saturation with respect to CO_2, the majority of the gas passes through to the surface. This relatively conservative behaviour of CO_2 makes it a better proxy of heat release from the shallow reservoir than chloride or measurement of observable heat flow (*Chiodini et al., 2005; Rissmann et al.,* 2011). The main error associated with any CO_2 based estimate of reservoir heat release is the correct estimation of CO_2 emission and the selection of a representative molar H_2O:CO_2 ratio. At RK we used a high spatial resolution to reduce the uncertainty in the CO_2 emission, and the concentration ratio of 16.6 is considered representative (as discussed in Section 5.3) and therefore the value of 315 ± 8 MW_t is considered representative.

Our data indicates that high spatial resolution φCO_2 surveys are sufficient or superior for constraining the heat and mass flows of hydrothermal systems compared to other mechanisms such as, soil temperatures, chloride flux or SO_2 emissions when used in conjunction with stable isotopic analysis of the soil gas in order to constrain the sources of φCO_2.

ACKNOWLEDGEMENTS

Thanks to GNS Science and GeoNet for the use of their equipment, Mighty River Power Limited, Powell Geoscience Ltd., University of Canterbury, D.O.C and Tauhara North No.2 Trust for access to the RK thermal area. This study contributes to and is funded by the UC-MRP Source 2 Surface research program. Additional

funding is from the Ministry of Science and Innovation's Foundation for Research, Science, & Technology through a TechNZ Scholarship and the University of Canterbury's Mason trust.

REFERENCES

Amundson, R., Stern, L., Baisden, T., Wang, Y., 1998. The isotopic composition of soil and soil-respired CO2. Geoderma, 82 (1-3), pp. 83-114. Http://dx.doi.org/10.1016/S0016-7061(97)00098-0

Bibby, H.M., Glover, R.B., Whiteford, P.C., 1995a. The Heat Output of the Waimangu, Waiotapu-Waikite and Reporoa Geothermal Systems (NZ): Do Chloride Fluxes Provide an Accurate Measure? Proceedings of the 17th NZ Geothermal Workshop. Pp 91-97.

Bibby, H.M., Caldwell, T.G., Davey, F.J., and Webb, T.H., 1995b. Geophysical evidence on the structure of the Taupo Volcanic Zone and its hydro-thermal circulation: Journal of Volcanology and Geothermal Research, v. 68, p. 29–58, http://dx.doi.org/10.1016/0377–0273(95)00007-H

Bowyer, D., and Holt, R., 2010, Case Study: Development of a Numerical Model by a Multi-Disciplinary Approach, Rotokawa Geothermal Field. Proc. World Geothermal Congress 2010 Bali, Indonesia, 25-29 April.

Cardellini, C., Chiodini, G., Frondini, F., 2003. Application of stochastic simulation to CO_2 flux from soil; mapping and quantification of gas release. J. Geophys. Res.108 (B9), 13

Chiodini, G., Cioni, R., Guidi, M., Raco, B., Marini, L., 1998. Soil CO 2 flux measurements in volcanic and geothermal areas. Appl. Geochem. 13, 543–552. http://dx.doi.org/ 10.1016/S0883-2927(97)00076-0

Chiodini, G., Granieri, D., Avino, R., Caliro, S., Costa, A., Werner, C., 2005. Carbon dioxide diffuse degassing and estimation of heat release from volcanic and hydrothermal systems. J. Geophys. Res. 110 (B8), 17. http://dx.doi.org/10.1029/2004JB003542

Chiodini G, Caliro S, Cardellini C, Avino R, Granieri D, Schmidt A, 2008. Carbon isotopic composition of soil CO2 efflux, a powerful method to discriminate different sources feeding soil CO2 degassing in volcanic-hydrothermal areas. Earth Planet Sci. Lett. 274:372–379. http://dx.doi.org/10.1016/j.epsl.2008.07.051

Collar, R.J. and Browne, P.R.L., 1985. Hydrothermal eruptions at the Rotokawa Geothermal Field, Taupo Volcanic Zone, New Zealand. Proc. 7th NZ Geothermal Workshop. . 1-5.

Dawson, G.B., 1964. The nature and assessment of heat flow from hydrothermal areas. N. Z. J. Geol. Geophys. 7, 155–171

Deutsch, C.V., Journel, A.G., 1998. GSLIB: Geostatistical Software Library and User's Guide. Applied Geostatistics Series. Oxford University Press, New York, Oxford.

Donaldson, I.G. and Grant, M.A., 1978. An estimate of the resource potential of New Zealand geothermal fields for power generation. Geothermics 7(2-4):243-52. http://dx.doi.org/10.1016/0375-6505(78)90014-7

Fridriksson, T., Kristjansson, B.R., Armannsson, H., Margretardottir, E., Olafsdottir, S., Chiodini, G., 2006. CO 2 emissions and heat flow through soil, fumaroles, and steam-heated mud pools at the Reykjanes geothermal area, SW Iceland. Appl. Geochem. 21, 1551–1569. http://dx.doi.org/ 10.1016/j.apgeochem.2006.04.006

Giammanco, S., Parello, F., Gambardella, B., Schifano, R., Pizzullo, S., Galante, G., 2007. Focused and diffuse effluxes of CO 2 from mud volcanoes and mofette south of Mt. Etna (Italy). J. Volcanol. Geotherm. Res. 165, 46–63. http://dx.doi.org/10.1016/j.jvolgeores.2007.04.010

Gregg, D.R., 1958. Natural heat flow from the thermal areas of Taupo Sheet District (N 94), New Zealand Journal of Geology and Geophysics, 1(1):65-75. http://dx.doi.org/10.1080/00288306.1958.10422795

Hedenquist, J.W., Mroczek, E.K., Giggenbach, W.F., 1988, Geochemistry of the Rotokawa Geothermal System: Summary of Data, Interpretation and Appraisal for Energy Development: DSIR Chemistry Division Technical Note 88/6, 64

Hochstein, M.P., Mayhew I., and Villarosa, R. A., 1990. Self-Potential Surveys of the Mokai and Rotokawa High Temperature Fields (NZ). Proceedings of the 12th NZ Geothermal Workshop.

Kerrick, D.M., 2001. Present and past non-anthropogenic CO_2 degassing from the solid earth. *Rev. Geophys.*, 39(4), 565–585. http://dx.doi.org/10.1029/2001RG000105

Krupp, R.E., and Seward, T.M., 1987. The Rotokawa Geothermal System, New Zealand: An Active Epithermal Gold-Depositing Environment. Economic Geology, 82(5):1109-1129. http://dx.doi.org/10.2113/gsecongeo.82.5.1109

Lewicki, J. L., Bergfeld, D., Cardellini, C., Chiodini, G., Granieri, D., Varley, N., & Werner, C., 2005. Comparative soil CO_2 flux measurements and geostatistical estimation methods on Masaya volcano, Nicaragua. *Bulletin of Volcanology*, *68*(1), 76-90. http://dx.doi.org/10.1007/s00445-005-0423-9

Lyon, G.L. and Hulston, J.R., 1984. Carbon and Hydrogen isotopic compositions of New Zealand geothermal gases. Geochemica & Cosmochimica Acta

48, 1161-1171. http://dx.doi.org/10.1016/0016-7037(84)90052-8

Mazot, A., Rouwet, D., Taran, Y., Inguaggiato, S., and Varley, N., 2011. CO_2 and He degassing at El Chichón volcano (Chiapas, Mexico): Gas flux, origin, and relationship with local and regional tectonics, Bull. Volcanol., 73, 423–441. http://dx.doi.org/10.1007/s00445-010-0443-y

Mörner, N.A., and Etiope, G., 2002. Carbon degassing from the lithosphere. Global Planet. Change 33, 185–203. http://dx.doi.org/10.1016/S0921-8181(02)00070-X

Rissmann, C.F., 2010. Using Surface Methods to Understand the Ohaaki Field, Taupo Volcanic Zone, New Zealand. Unpubl. Doctoral Dissertation. Univ. Canterbury, Christchurch, New Zealand.

Rissmann, C., Nicol, A., Cole, J., Kennedy, B., Fairley, J., Christenson, B., Leybourne, M., Milicich, S., Ring, U., Gravley, D., 2011. Fluid flow associated with silicic lava domes and faults, Ohaaki hydrothermal field, New Zealand. J. Volcanol. Geotherm. Res. 204, 12–26. http://dx.doi.org/10.1016/j.jvolgeores.2011.05.002

Rissmann, C., Christenson, B., Werner, C., Leybourne, M., Cole, J., Gravley, D., 2012, Surface heat flow and CO 2 emissions within the Ohaaki hydrothermal field, Taupo Volcanic Zone, New Zealand, Appl. Geochemistry 27, 223-239. http://dx.doi.org/10.1016/j.apgeochem.2011.10.006

Rowland, J.V. and Sibson, R.H., 2004. Structural controls on hydrothermal flow in a segmented rift system, Taupo Volcanic Zone, New Zealand. Geofluids 4:259–283. http://dx.doi.org/10.1111/j.1468-8123.2004.00091.x

Seward, T.M., and Kerrick, D.M., 1996. Hydrothermal CO_2 emission from the Taupo Volcanic Zone, New Zealand. Earth Planet. Sci. Lett., 139, 105–113. http://dx.doi.org/10.1016/0012-821X(96)00011-8

Sheppard, D.S., Faivre-Perriet, R.X., Orange, C.J., Le Guern, F., 1990. Soil gas surveys: A cheaper alternative to geophysical surveys: Three examples from the Taupo Volcanic Zone. Proceedings of the 12th NZ Geothermal Workshop.

Sinclair, A.J., 1974. Selection of thresholds in geochemical data using probability graphs. J. Geochem. Explor. 3, 129–149.

Thompson, S.K., 1990. Adaptive cluster sampling. J. Am. Stat. Assoc. 85, 1050-1059. http://www.jstor.org/stable/2289601

Welles, J.M., Demetriades-Shah, T.H. and McDermitt, D.K., 2001. Considerations for measuring ground CO_2 effluxes with chambers. Chemical Geology, 177(1-2): 3-13. http://dx.doi.org/10.1016/S0009-2541(00)00388-0

Werner, C., Brantley, S.L., Boomer, K., 2000. CO_2 emissions related to the Yellowstone volcanic system. 2. Statistical sampling, total degassing, and transport mechanisms. J. Geophys. Res. 105, 10,831–10,846.

Werner, C., Hochstein, M.P., Bromley, C.J., Manville, V.R., Tilyard, D., 2004. CO_2-flux of steaming ground at Karapiti (Wairakei, NZ). Geol. Soc. N. Z. 117A, 115–116

Werner, C., Cardellini, C., 2006. Comparison of carbon dioxide emissions with fluid upflow, chemistry, and geologic structures at the Rotorua geothermal system, New Zealand. Geothermics 35, 221–238. http://dx.doi.org/10.1016/j.geothermics.2006.02.006

Werner, C., Hurwitz, S., Evans, W.C., Lowenstern, J.B., Bergfeld, D., Heasler, H., Jaworowski, C., Hunt, A., 2008. Volatile emissions and gas geochemistry of Hot Spring Basin, Yellowstone National Park, USA. Journal of Volcanology and Geothermal Research, 178 (4), pp. 751-762. http://dx.doi.org/10.1016/j.jvolgeores.2008.09.016

Winick, J., Powell, T., Mroczek, E., 2011. The natural-state geochemistry of the Rotokawa reservoir. Proceedings of the 33rd NZ Geothermal Workshop. 16-18 November.

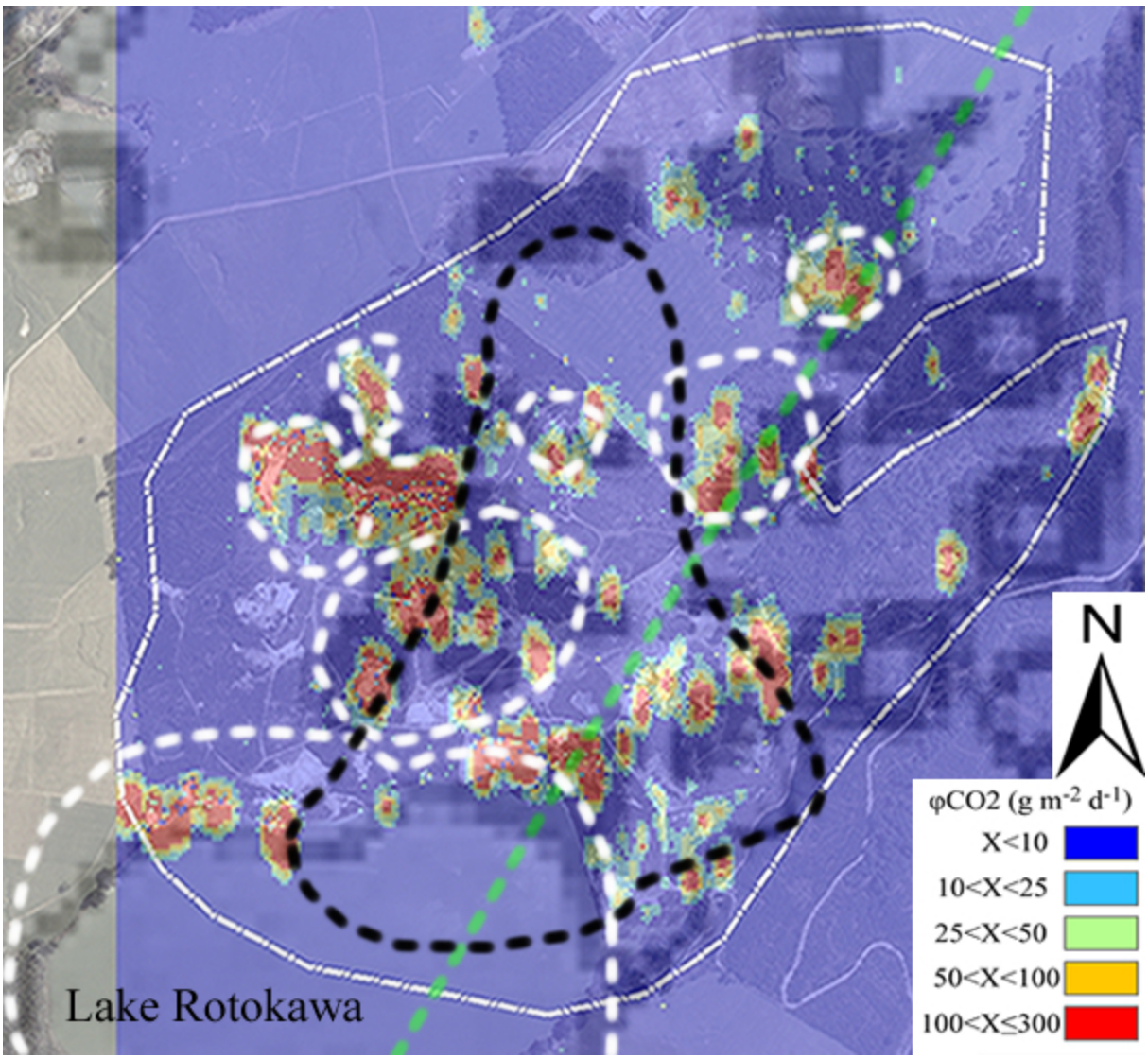

Figure 7: Full Field sGs model of φCO_2. Black Line is the 200mV contour from *Hochstein et al.*, 1990. White Dash Lines are historic hydrothermal eruption craters from *Krupp & Seward*, 1987. Green dashed line is the CFF from *Winick et al.*, 2011. Dark areas in the background are heat anomalies from *Gregg*, 1958.